

Molecular arrangements of self-assembled surfactant films: Characterization from atomic force microscopy data

O. Teschke^{1,*} and E. F. de Souza²¹*Nano-Structure Laboratory, IFGW/UNICAMP, 13081-970 Campinas, SP, Brazil*²*Faculdade de Química-CEATEC, Pontificia Universidade Catolica de Campinas, 13086-900 Campinas, SP, Brazil*

(Received 11 October 2002; revised manuscript received 30 April 2003; published 3 September 2003)

The adsorbed surfactant film molecular arrangement with thickness of ~ 5 nm is determined by measurements of the film dielectric permittivity. Before the advent of atomic force microscopy the dielectric permittivity was a macroscopic parameter, appropriate only for describing uniform environments since its profile was difficult to measure for local intermolecular interactions and its spatial distribution was frequently settled without experimental justification. Here, we show that atomic force microscopy made it possible to measure the dielectric permittivity profile in a scale below 5 nm for adsorbed layers of self-assembled surfactant films in water. The measured values of the film's dielectric permittivity and the film's thickness determine the compactness of the adsorbed film and consequently the presence of water molecules in the film and the conformal structure of the adsorbed molecules.

DOI: 10.1103/PhysRevE.68.031401

PACS number(s): 82.70.Dd, 81.05.Zx, 77.22.Ch, 77.55.+f

I. INTRODUCTION

The structural and dynamic properties of adsorbed molecular films are of both fundamental and applied interest in diverse areas, such as statistical mechanics of complex fluids and thin-film boundary lubrication and coatings, and have been the subject of recent experimental and theoretical investigations [1–3]. A large number of molecular processes in chemical, physical, and biological related systems occur at solid/liquid or liquid/liquid interfaces. The presence of an interface has been shown to modify the dynamical behaviors of molecules relative to their bulk properties [4]. These modifications influence reaction kinetics and photochemical processes. When properties of these systems are measured within distances comparable with molecular lengths, fundamental differences between the response of the liquid under geometrical restriction and the bulk are observed [5].

Clearly, how an adsorbed surfactant molecule modifies the surface properties of a substrate is a subject of great importance, and it certainly must depend on the orientation and conformation of the surfactant adsorbed molecules [6]. Understanding the adsorption mechanism of surfactant molecules at the solid/liquid interface is an important step toward modeling industrial processes which use surfactants on a large scale, such as detergency, water purification, oil recovery, and ore refinement by flotation [7]. An intermolecular interaction in bulk solution leads to a variety of surfactant self-assembled structures such as micelles which have been well studied [8]. At an interface, however, the normal self-assembly process is perturbed by competing surfactant-surface and solvent-surface interactions [9]. Over the past few decades, the adsorption characteristics of a wide variety of surfactant-solvent-substrate systems have been investigated, traditionally by adsorption isotherm [10] and more recently by fluorescence decay [11] and neutron reflection [12].

So far, however, little is known because traditional surface techniques are incapable of providing much information on the problem of determining the orientation and conformation of the surfactant adsorbed molecules [13]. Among the techniques recently used is the infrared-visible sum-frequency vibrational spectroscopy which was used to obtain information about the orientation and conformation of dioctadecyl dimethyl ammonium chloride surfactant adsorbed at solid surfaces [6]. Monolayers of sodium bis(2-ethylhexyl)sulfosuccinate are studied by neutron reflectivity, and from this data the authors proposed the head group and the hydrocarbon chains thicknesses which are compared with the theoretical molecular length [14]. Techniques such as fluorescent probes or ellipsometry provide evidences for the existence of molecular aggregates on solid substrates, although they are not able to directly determine the geometry of these aggregates [15].

Imaging hard samples with atomic resolution requires a probe with atomic dimensions. The atomic force microscope (AFM) obtains its topographical information from short-range repulsion resulting from the overlap of electronic shells between tip and sample [16]. However, the presence of long-range interactions such as the double layer electrostatic force [17–21] when scanning soft samples in liquid media leads to a very different imaging scenario.

In this work, we explore the surfactant adsorbed structure in the interfacial region by measuring the force acting on the tip when immersed in self-assemblies of surfactant films at the interface between an aqueous solution and a substrate. For this purpose, AFM topographic views and force curves were used to characterize structurally different adsorbed layers. The contributions of surfactant and surface charges, hydrophobic tail, and water dipoles located within the interface to the effective electrostatic interaction energy and the effect of the dielectric permittivity gradient on local interfacial electrostatics are described. The molecular structural distribution is based on the calculated dielectric permittivity profile within the surfactant layer.

*Electronic address: oteschke@ifi.unicamp.br

Previous interfacial force measurements using atomic force microscopy

Previous force vs distance measurements by AFM using tips made of silicon nitride (Si_3N_4) and mica substrate have been reviewed by Capella and Diether [22]. Calibration, noise, and systematic errors are discussed in detail [23]. The first results were obtained by Butt [24], then by Weisenhorn *et al.* [25], and later by Atkins and Pashley [26]. In order to eliminate the problem of the unknown shape of the tip, various studies [22] have used modified cantilevers with tips of known geometry. Measurements of colloidal forces using AFM were reported by Ducker *et al.* [27]. Later Jaschke *et al.* [28] used AFM to study surface properties. Adsorbed layer structure of surfactants on quartz was investigated by Schulz *et al.* [29]. Fleming and Wanless [30] outlined the soft imaging techniques to characterize the adsorption of surfactants and polymers at the solid/liquid interface.

Therefore early studies were unable to explore the microstructure of surface aggregates. In the past few years, AFM was used to directly visualize the structure of aggregates formed on a variety of surfaces and under various solution conditions. For instance, AFM images of surfactants adsorbed in hydrophobic graphite were interpreted to be low surface density adsorbed monolayers with the surfactant molecules oriented such that only tails are in contact with the surface or also more elaborated geometrical forms such as hemicylinders or mixtures of hemicylinders and lamellae [20,31–35]. AFM experiments with hydrophilic surfaces such as silica and mica have shown structures such as full spheres, full cylinders, and bilayers. But the AFM studies mentioned above were all conducted at surfactant concentrations well above the bulk critical micellar concentration (CMC), while the critical aggregate concentration (CAC) corresponding to the formation of surface aggregates is typically one to four orders of magnitude lower than the bulk CMC. Therefore, it is possible that the equilibrium aggregates which exist on the surface at concentration near CAC can have microstructures that deviate significantly from those seen via AFM at high surfactant concentrations. In fact, Johnson and Nagarajan [36] used the calculated equilibrium free energy for the formation of a given structure to model the self-assembly of surfactants at hydrophilic solid/liquid interface and showed that the formation of monolayers and bilayers were favored. In both cases, the monolayers or the inner layer of a bilayer, the surfactant molecules of are oriented such that their head groups are in contact with the hydrophilic surface. Composite structures such as hemicylindrical or hemispherical patterns on the hydrophobic monolayer assembled over the hydrophobic surface are only obtained as the surfactant concentration is increased [37].

II. EXPERIMENT

With the advent of Si_3N_4 supertips, the tip/substrate interaction configuration was radically altered. The details of the interaction [38] and the experimental setup was described previously [39–41]. Images were obtained in surfactant solutions at room temperature ($\sim 25^\circ\text{C}$) by a commercial AFM (TopoMetrix TMX2000, ThermoMicroscope). The fol-

lowing surfactants were used: dioctadecyl dimethyl ammonium bromide ($2\text{C}_{18}\text{DAB}$), hexadecyl trimethyl ammonium bromide (C_{16}TAB), tetradecyl trimethyl ammonium bromide (C_{14}TAB), dodecyl trimethyl ammonium bromide (C_{12}TAB), and hexadecyl pyridinium bromide (CPBr). Surfactants were purchased from Aldrich and used as supplied, without further purification; solutions made of water [milli-Q gradient quality, resistivity $\sim 18.2\text{ M}\Omega/\text{cm}$, total organic carbon (TOC) $< 5\text{ ppb}$ (parts per billion)] were introduced into the cell after the substrate was mounted on the xyz translator of the AFM. Surfactant adsorption was accomplished by merely introducing an aqueous solution of the surfactant into the fluid cell and allowing the freshly cleaved mica to stand in this solution for approximately $\sim 1\text{ h}$ before operation. Both unmodified silicon nitride (Si_3N_4) tips ($\epsilon_T = 7.4$) and tips etched in 50% w/w HF solutions for 10 min before operation were used. Measurements started $\sim 15\text{ min}$ after the tip was immersed in the solution. The surface of a Si_3N_4 tip in aqueous solution is composed of amphoteric silanol and basic silylamine (secondary and/or primary amines, though the latter is rapidly hydrolyzed) surface groups [42], at $\text{pH} \sim 6$. With no added electrolyte, the Si_3N_4 surface is either *zwitterionic* (zero net charge) or slightly negatively charged [43]; Lin *et al.* reported that the surface potential of the Si_3N_4 tip is nearly zero at $\text{pH} = 6.0$ [44]; consequently, we assumed that the surface charge density in the tip $\sigma_{\text{Tip}} \ll \sigma_{\text{Mica}}$. When the mica basal plane is placed in water, the mechanism for the formation of the double layer is assumed to be the dissolution of K^+ ions as well as the exchange of K^+ by H^+ or H_3O^+ ions. When surfactant is added to water, K^+ ions are also substituted by $(\text{C}_{18}\text{H}_{37})_2(\text{CH}_3)_2\text{N}^+$ ions in ($2\text{C}_{18}\text{DAB}$) solutions, $(\text{C}_{16}\text{H}_{33})(\text{CH}_3)_3\text{N}^+$ in (C_{16}TAB) solutions, $(\text{C}_{12}\text{H}_{25})(\text{CH}_3)_3\text{N}^+$ in (C_{14}TAB) solutions, $(\text{C}_{12}\text{H}_{25})(\text{CH}_3)_2\text{N}^+$ in (C_{12}TAB) solutions and $(\text{C}_{16}\text{H}_{33})(\text{C}_5\text{H}_6\text{N}^+)$ in CPBr solutions. The concentrations used in this work are lower than the critical micellar concentration (CMC) (see Table I), but also at concentrations much lower than CMC there is adsorption at the solid/liquid interface and the formation of premicelles detected by electrical conductivity measurements.

III. EXPERIMENTAL RESULTS

Figure 1 shows different sizes of adsorbed aggregates forming islands, agreeing with reported results that upon extended exposure CTAB molecules aggregate to form islands on the mica surface [45]. In order to determine the film thickness, force vs separation curves at background (region I) and islands (region II) were measured. The results are shown in Fig. 2 where two different regions (I and II) show distinct force vs separation curves [curve W_I measured at the background (Δ for $v = 1\ \mu\text{m/s}$) and curve W_{II} measured at the islands (\square for $v = 1\ \mu\text{m/s}$), where v is the tip/substrate approach velocity].

Control experiment curves were measured using Si_3N_4 tips immersed in the milli-Q plus water-mica double layer. One of the force vs separation control curves is shown by curve \circ in the inset of Fig. 2(a). Also in Fig. 2, curves W_I

TABLE I. Surfactant molecules adsorbed layer properties.

Surfactant	CMC (<i>M</i>)	<i>n</i>	Calculated molecular length (nm)	Calculated thickness (nm)	Measured thickness (nm)	Measured rupture force (nN)	ϵ^a
C ₁₂ TAB bilayer	$1.46 \times 10^{-2}{}^b$	12	1.5	3.0	2.9 ± 0.01	0.2 ± 0.03	2 ± 0.5
C ₁₄ TAB bilayer	$3.54 \times 10^{-3}{}^c$	14	1.8	3.6	3.3 ± 0.01	0.5 ± 0.03	2 ± 0.5
C ₁₆ TAB monolayer	$8.9 \times 10^{-4}{}^d$	16	2.0	2.0	2.3 ± 0.01	0.8 ± 0.03	36 ± 0.5
C ₁₆ TAB bilayer	$8.9 \times 10^{-4}{}^e$	16	2.0	4.1	3.6 ± 0.01	0.3 ± 0.03	4 ± 0.5
2C ₁₈ DAB monolayer	$1.0 \times 10^{-5}{}^f$	18	2.3	2.5	2.5 ± 0.01^i	0.7 ± 0.03	2 ± 0.5
CPBr bilayer I	$6.7 \times 10^{-4}{}^g$				3.1 ± 0.01	0.5 ± 0.03	3.3 ± 0.5
CPBr bilayer II	$6.7 \times 10^{-4}{}^h$				3.1 ± 0.01	0.3 ± 0.03	2.6 ± 0.5
CPBr			Uncovered region				

^aDielectric constant value estimated using the values reported for other surfactant molecules [*Handbook of Chemistry and Physics*, 66th ed. (CRC Press, Boca Raton, 1985), E-52].

^bV. Mosquera, J.M. del Rio, D. Attwood, M. Garcia, M.N. Jones, G. Prieto, M.J. Suarez and F. Sarmiento, *J. Colloid. Interface Sci.* **206**, 66 (1998).

^cR. Zielinski, S. Ikeda, H. Nomura, and S. Kato, *J. Chem. Soc. Faraday Trans. 1* **84**, 151 (1988).

^dJ.N. Phillips, *Trans. Faraday Soc.* **51**, 561 (1955).

^eH.V. Tartar, *J. Colloid Sci.* **14**, 115 (1959).

^fP. Mukerjee and K.J. Mysels, in *Critical Micelle Concentrations of Aqueous Surfactant Systems*, Nat. Bur. Stand. Ser. No. 36 (U.S. GPO, Washington, D.C., 1971).

^gN.M. Van Os, J.R. Haak, and L.A.M. Rupert, *Physico-Chemical Properties of Selected Anionic, Cationic and Nonionic Surfactants* (Elsevier, Amsterdam, 1993).

^hD.F. Evans and P.J. Wightman, *J. Colloid Interface Sci.* **86**, 515 (1982).

ⁱMonolayer, unmarked bilayers.

and W_{II} show that in $5 \times 10^{-5} M$ C₁₆TAB surfactant solutions, the attraction and repulsion long-range components are displaced by the surfactant layer thicknesses indicated by W_I and W_{II} when compared to the curve in water [curve \circ in the inset of Fig. 2(a)]. At (2.3 ± 0.1) nm from the surface in region I [curve \triangle in Fig. 2(a)], there is a rapid change in force with a small change in tip/surface separation. The value

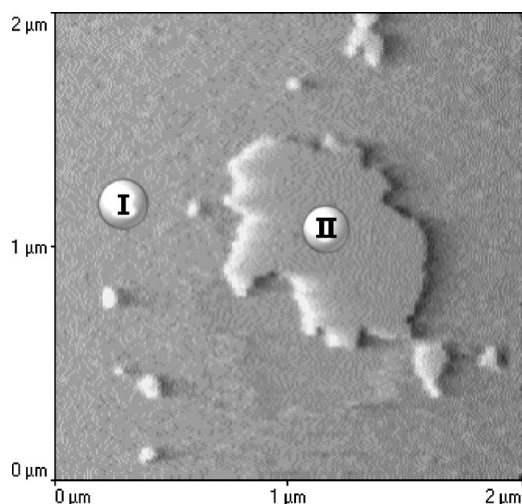


FIG. 1. AFM image of a C₁₆TAB adsorbed layer on mica in $5 \times 10^{-5} M$ C₁₆TAB solutions. The islands (patches, region II) indicate higher structures than the background (region I) in agreement with the standard contrast shown by AFM images.

of overall thickness of this layer is consistent with the formation of monolayers (the length of the fully extended molecule being about 2.2 nm). With sufficiently large applied force (~ 0.8 nN), the surfactant layer is removed from the space between the tip and the surface.

A different force curve is observed at region II [Fig. 2(b)]. The large repulsive deviation from the exponential component, starting at (4.4 ± 0.1) nm from contact, is followed by an attraction regime at ~ 3.2 nm, which corresponds to the thickness of a bilayer.

Molecules forming thin layers are expected to be easily pushed away from the contact zone compared to the ones forming thick layers, but the opposite is observed [compare Figs. 2(a) and 2(b)].

The adsorbed layer thicknesses of surfactants C_{*n*}TAB (where *n* corresponds to the number of carbon atoms in the hydrophobic tail) with various hydrophobic tail lengths were measured. The measured bilayer thicknesses and the calculated extended molecular lengths using the expression $l_{max} \sim (0.15 + 0.1265n)$ [8], where *n* is the number of carbon atoms, are shown in Table I.

Analogous to C₁₆TAB adsorbed layer images, adsorbed 2C₁₈DAB images show that molecules aggregate to form islands on the mica surface. In order to determine the film thicknesses, force vs separation curves at the islands and outside were measured. The measured curve shows that, in 2C₁₈DAB surfactant solutions, at 2.5 nm from the surface, there is a rapid change in force with a small change in tip/surface separation. The thickness of this layer is consistent

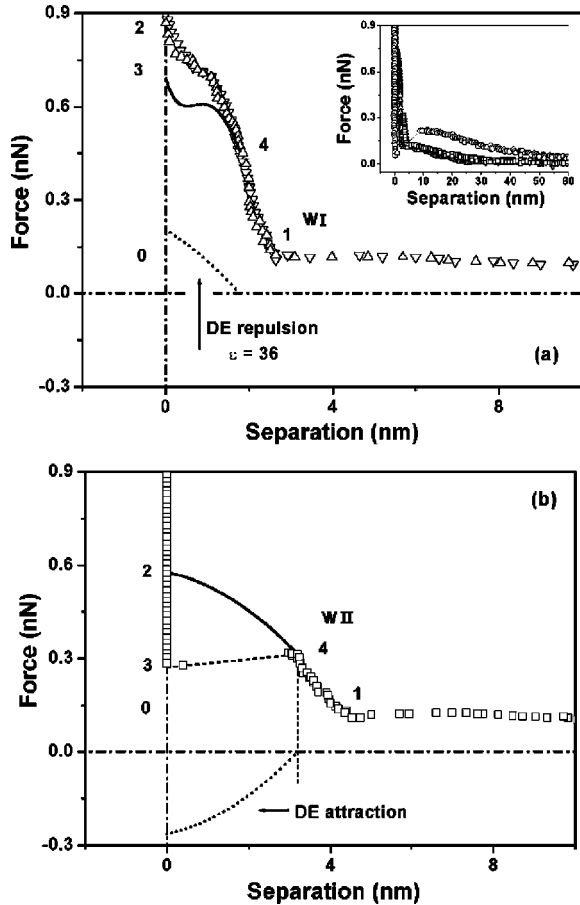


FIG. 2. Force vs separation curves measured for the $C_{16}TAB$ adsorbed layer on mica in $5 \times 10^{-5}M$ solutions. (a) Background region and (b) islands. The DEF acting on the tip when immersed in surfactant layer, calculated for a tip with a spherical end with $R \approx 5$ nm, indicated by the dotted line.

with the formation of monolayers (the length of the fully extended molecule being about 2.3 nm). Force vs separation curves observed at the region outside the islands are identical to the control experiment measured curves performed using mica in water. So in $2C_{18}DAB$ solutions the surface is covered only by monolayers and part of the surface is uncovered: no bilayers of $2C_{18}DAB$ were observed.

Figure 3 shows measured force vs separation curves in $5 \times 10^{-3}M$ CPBr surfactant solutions. The repulsive long-range component length (Debye length) is substantially reduced due to the high concentration of the surfactant solution when compared to curves measured in $10^{-5}M$ solutions. The surfactant layer thickness is indicated by W_I ; curves \circ and \bullet were measured at two different regions of the covered surface. The value of overall thickness of these layers is consistent with the formation of monolayers (the length of the fully extended molecule being about 2.2 nm). At sufficiently large applied forces (~ 0.6 nN and ~ 0.4 nN for curves \circ and \bullet , respectively), the surfactant layer is removed from the space between the tip and the surface.

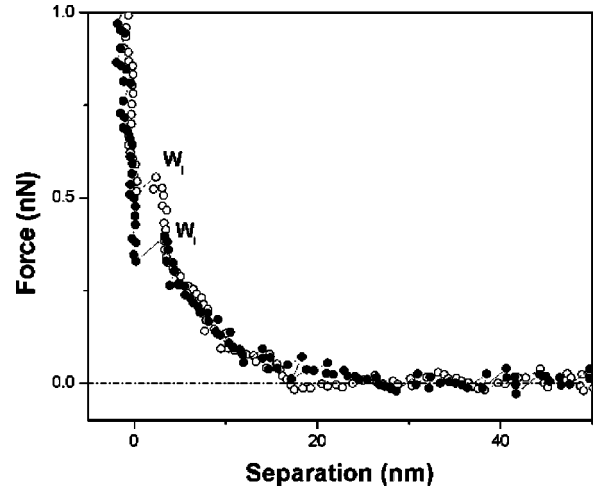


FIG. 3. Force vs separation curves measured for the CPBr adsorbed layers on mica in $5 \times 10^{-3}M$ solutions: region (a) is indicated by \circ and region (b) is indicated by \bullet .

IV. DIELECTRIC EXCHANGE FORCE MODEL: WATER/MICA INTERFACE

Let us now concentrate on the control experiment that was performed in pure water (with a dielectric permittivity $\epsilon \approx 80$ in the bulk) in order to characterize the mica interface in the absence of adsorption layers. Forces acting on the tip when immersed in the region close to interface [curve \circ in the inset of Fig. 2(a)] were previously discussed [23]. A simple analytical expression for the electrostatic force was previously derived [38,46] for a tip immersed in the mica double layer in water. The tip was defined to have a sharpened conical shape with a cone angle $\alpha = 18^\circ$ and a flat end with radius R (microlever type *B* park). The displacement vector is assumed to have an exponential spatial dependence $D(z) = D_0 \exp(-\kappa z/2)$, where D_0 is determined by the ionic charge distribution at the mica surface by using Gauss' Law. The elemental volume (dv) of the tip immersed in the double layer region is given by $dv = \pi[R + z \tan\alpha]^2 dz$, where z is the integration variable of the trapezoidal volume and H is the distance between the surface and the end of the tip. The electric energy variation involved in the exchange of the dielectric permittivity of the double layer by that of the immersed tip volume in the double layer region. The force is obtained by the gradient of the energy expression, i.e.,

$$F_z = -(\partial/\partial z)\Delta E, \text{ where}$$

$$\Delta E = \frac{1}{2\epsilon_0} \int_0^{10\kappa^{-1}-H} \left[\frac{1}{\epsilon_{tip}} - \frac{1}{\epsilon_{DL}(z)} \right] D^2(z) dv. \quad (1)$$

In the London dispersion account describing the intermolecular interaction, a frequency-dependent isotropic polarizability $\alpha(\omega)$ is calculated. Here we phenomenologically have assumed a spatially variable dielectric permittivity

$\epsilon(z)$, which is calculated by adjusting the $\epsilon(H)$ profile to the force vs separation curve close to the interface (≈ 100 nm) using Eq. (1).

To compare experiments with calculations, we have fitted the repulsive part of the force vs separation curves with the gradient of Eq. (1). Initially, by substituting ϵ_{DL} for ϵ_{bulk} , we fitted the repulsive part of the curve where the adjustment parameters κ^{-1} and D_0 are determined. Then, by adjusting the parameters in the ϵ_{DL} expression it is possible to fit the attraction part of the curve. The pure water dielectric permittivity value at the mica interface that results in the best fitting of the experimental curve [\circ in the inset of Fig. 2(a)] is ~ 4 , in agreement with the value of 4.2 given in Ref. [47] and in our work [48].

V. DIELECTRIC EXCHANGE FORCE MODEL: WATER/SURFACTANT/MICA INTERFACE

In order to explain the unexpected result that thin surfactant layers (background, region I in Fig. 1) show higher rupture forces than thick layers (islands, region II in Fig. 1), we have proposed that a distinct force component than the force associated with steric limitations imposed by the immobilization of $C_{16}TAB$ and by the location of $C_{16}TAB$ binding site at the mica surface [45] acts on the tip when it is immersed in the surfactant layer. Attraction or repulsion present when the tip is immersed in thin or thick surfactant layers is associated with dielectric permittivity of the surfactant layer and tip. To support our claims, the force component, when the tip is immersed in the surfactant layer, was calculated using Eq. (1), assuming a half-spherical shape for the lower tip surface, since only its spherical part, with elemental volume $dv = \pi[R^2 + (R-z)^2]dz$, is immersed in the surfactant layers for $R \sim 5$ nm and $W \sim 3$ nm.

The effect of the dielectric exchange force (DEF) when the tip is immersed in the region covered by a layer forming the background will be discussed first. The energy spent by approaching the tip to the interface corresponds to the area covered by the triangle (0-1-2) in Fig. 2(a); part of this energy will be fitted to the calculated energy associated with the force involved in the tip immersion in the surfactant layer with an adjustable value of the dielectric permittivity. The result is shown by the dotted line in Fig. 2(a), indicated as "DE repulsion." This energy component is subtracted from the experimental curve and the result is shown by the line 3-4. The value of ϵ that best fitted this region is ≈ 36 . This value agrees with the published ones for the dielectric permittivity of $C_{16}TAB$ solutions at CMC [49].

The energy associated with the immersion of the tip in the thick layer is shown by the area indicated by "DE attraction," in the lower part of the force vs separation curve [Fig. 2(b)]. If this negative component is added to the original measured curve, we obtain a curve similar to the one measured when the tip is immersed in the thin layer, indicating that our fitting of the experimental curve is a reasonably calculated value of the attraction component. Consequently, the DEF gives a consistent description of the distinct force vs separation curves measured when the tip is immersed in a surfactant layer by assuming a thick layer with a dielectric

permittivity ~ 4 and a thin layer with $\epsilon \approx 36$.

At a sufficiently large applied force, the surfactant layer is squeezed from the space between the tip and the surface. This value is defined as the film rupture force and it is equal to ~ 0.8 nN for the background region and ~ 0.3 nN for the islands. The results shown in the previous paragraphs demonstrate that the DEF accounts for the difference in the rupture force of the two layers with different thicknesses and dielectric permittivities.

What is then the structure of the surfactant near the mica/surfactant solution boundary? As the tip and mica surfaces separated by a water layer were pushed together, fluid drained smoothly until forces of alternate repulsion and attraction were first detected at thickness ~ 4.6 nm. These forces arise from the tendency of the surfactant to form layers on the surface. Does this response reflect a static structure perhaps induced by the walls or by molecular packing or was it induced by shearing? Although shearing may have contributed, it is experimentally clear that we have identified two qualitatively different responses to the tip approach of these surfactant film's patches or aggregates and background. Our results also show that patches (bilayers) are formed at mica sites with a concentration as low as $5 \times 10^{-5} M$.

VI. ADSORBED MOLECULAR ARRANGEMENT DETERMINATION BY THE DIELECTRIC PERMITTIVITY PROFILE AND FILM THICKNESS

This work describes the force acting on AFM tips when immersed in the surfactant adsorbed layer. Measurements with a spatial resolution of ± 0.01 nm determine the magnitude of the relative dielectric permittivity value $\epsilon_{relative}$ with resolution ± 0.5 . This task is accomplished by modeling the force acting on the tip during its immersion in the surfactant layer by the DEF. This force calculation assumes a variable dielectric permittivity of the adsorbed layer. The dielectric permittivity measured value is compared to the value measured at CMC and the dielectric permittivity of water around $\epsilon \approx 80$. More compact configuration implies in a measured value close to $\epsilon \approx 2$, while less compact structures will contain water molecules and the value of ϵ is substantially increased. The combination of the measured values of the dielectric permittivity with a resolution of $\Delta\epsilon \approx 0.5$ and the film thickness with a resolution of 0.01 nm indicates the conformal structure of the adsorbed molecules. AFM images are also capable of revealing the topology of the surfactant/solution interface and the distance from that interface to the solid surface, which are comparable to the surfactants molecular lengths.

The surfactant molecular arrangement for $C_{16}TAB$ determination is as follows. By comparing the extended length of the surfactant molecules to the measured thickness of the adsorbed layers and knowing that the substrate is charged, it is possible to determine the spatial distribution of the molecules in the direction normal to the substrate, for example the monolayer shown in Fig. 4(c) or bilayer shown in Fig. 4(a). By measuring the dielectric permittivity, it is possible to determine the compactness of the layer, for example, the amount of water the layer contains or how close is the mol-

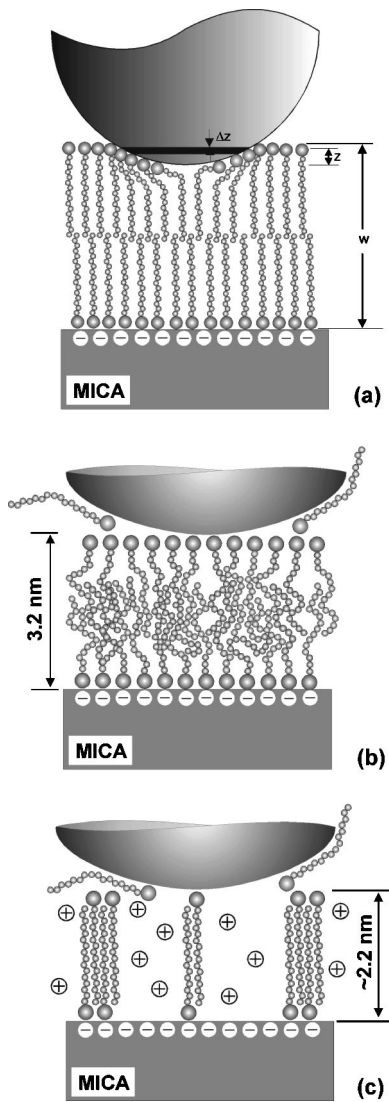


FIG. 4. Bilayer molecular structure of the adsorbed C_{16} TAB layer on a mica surface. (a) Tip/surfactant/substrate interaction region, where a tip with a sphere end and a radius R is immersed in the surfactant layer region, z is the integration variable of the elemental volume with a width Δz , and d is the distance between the surface and the end of the tip. The highly compact molecular arrangement with a measured dielectric permittivity equal to ~ 4 and a thickness of 4.4 nm. (b) The probable molecular structure of the adsorbed C_{16} TAB layer before rupture with a measured thickness of ~ 3.2 nm. (c) Monolayer with $\epsilon \approx 36$ and a thickness of 2.3 nm.

ecule with its neighbors as shown in Figs. 6(a) and 6(b). Lower values of the measured dielectric permittivity imply in more compact layers, as shown by the comparison of Figs. 6(a) and 6(b).

As in previous studies, mica surfaces immersed in $5 \times 10^{-5} M$ C_{16} TAB concentrations solutions were found to be not completely covered, lending support to the idea that absorption is in the form of aggregates. These aggregates or islands have a 3.2 nm overall thickness before rupture and strongly resemble bilayer fragments, as previously reported [50]. The evidence for bilayer formation presented in this work at region II is conclusive, since the measured thickness

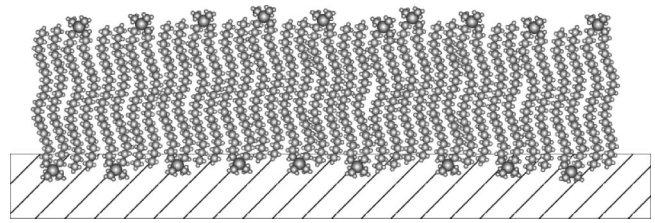


FIG. 5. Probable $2C_{18}$ DAB molecular configuration at an interface showing an adsorbed monolayer.

before rupture is 3.2 nm and a dielectric permittivity value of $\epsilon \approx 4$ was measured. Thus, at region II the adsorbed layer film is formed by a more compact molecular arrangement; these aggregates have extended sufficiently to form bilayer structures shown in Fig. 4(a), and the molecular configuration before rupture is shown in Fig. 4(b).

The measured value of the dielectric permittivity of $\epsilon \approx 36$ for the thin adsorbed layer region (which correspond to the monolayer) indicates that there is a significant fraction of water in this layer, associated with the high value of the dielectric constant. The probable configuration of the surfactant molecules in this layer is shown in Fig. 4(c). Force vs separation curves are then particularly useful for discriminating between monolayer and bilayer formation, since both the thickness and dielectric permittivity of the structure are simultaneously measured.

Dielectric permittivity was also calculated by fitting the force vs distance curves to the DEF expression for C_{12} TAB and C_{14} TAB surfactant layers. The value of dielectric permittivity that best fitted the experimental curves is $\epsilon \approx 2$ for both C_{12} TAB and C_{14} TAB.

The next surfactant molecular structure that will be discussed is formed by $2C_{18}$ DAB molecules which have two hydrophobic tails. Patches are formed on the surface, similar to the adsorbed structure formed when mica is immersed in a C_{16} TAB solution. Fitting the force vs separation curve to Eq. (1) for the covered region gives the value that results in the best fitting for the attraction component $\epsilon \approx 2$, for a layer thickness of ~ 2.4 nm. This corresponds to a very compact layer of surfactant and since the surfactant molecule extended length is ~ 2.3 nm, it corresponds to a monolayer. Since the layer thickness corresponds to a monolayer and $\epsilon \approx 2$, the most probable molecular configuration is shown in Fig. 5 which depicts the possible arrangement of the $2C_{18}$ DAB molecules in a mica/water interface. Contrary to the pattern formed by C_{16} TAB adsorbed molecules, $2C_{18}$ DAB adsorbed molecules do not form bilayers.

VII. MOLECULAR ARRANGEMENT CORRESPONDING TO ADSORBED CPBR

Figure 6 shows the force vs separation curves for mica immersed in $5 \times 10^{-5} M$ CPBr solutions. Two different force vs separation curves were observed and are shown in Figs. 6(a) and 6(b). Observe that the width of the repulsion layers is equal and corresponds to the thickness of an adsorbed bilayer. Consequently in CPBr solutions, we have observed only bilayer patches on the surface and an uncovered region.

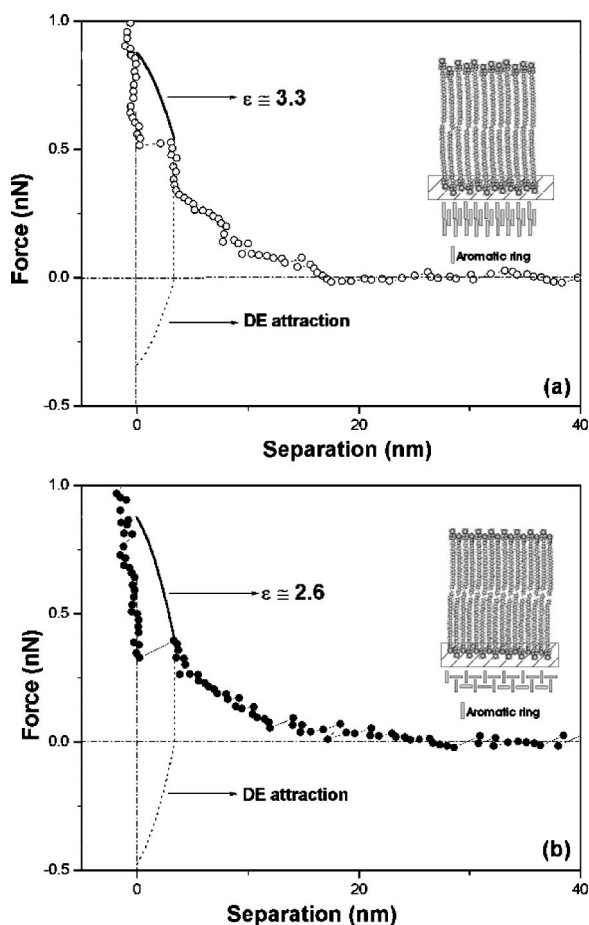


FIG. 6. Force vs separation curve measured in $5 \times 10^{-3} M$ CPBr solutions. The DEF acting on the tip when immersed in the surfactant layer, calculated for a tip with a spherical end with $R \approx 5$ nm and using Eq. (1), indicated by the dotted line. (a) for $\epsilon \approx 3.3$. Inset: Probable molecular configuration of the CPBr adsorbed layer at the mica interface and (b) the same as in (a) for $\epsilon \approx 2.6$.

However, the two regions show different rupture forces, indicating that a similar molecular distribution with the same layer width (3.4 nm) but distinct dielectric permittivities is present at the interface. The probable surfactant layer configurations are schematically shown in the inset of Figs. 6(a) and 6(b); the molecular arrangement bars indicate aromatic rings. The inset of Fig. 6(a) shows the configuration corresponding to a distribution where the aromatic rings occupy a larger area per molecule than the one shown in the inset of Fig. 6(b). The molecular arrangement that results in a very packed configuration is shown in Fig. 6(b) and corresponds to a measured value of $\epsilon \approx 2.6$. These arrangements are based on the fact that in configuration shown in Fig. 6(a) the repulsion between π electrons in the aromatic rings is minimized since nearest neighbor rings are at 90° from each other, consequently the configuration is more compact than the one shown in Fig. 6(a). We also have assumed that the less compact arrangement in Fig. 6(a) may reorient the molecular arrangement more easily than the more compact one in Fig. 6(b), resulting in different values of dielectric permittivity for the two configurations.

VIII. DISCUSSION OF THE TECHNIQUE

The adsorption characteristics of a wide variety of surfactant-solvent-substrate systems have been investigated, traditionally by adsorption isotherm [10] and more recently by fluorescence decay [11] and neutron reflection [12]. Laser and synchrotron radiation measurements probe the details of the structure at the interface averaging measurements in an area corresponding to the beam area. The detected roughening of the interface by thermal fluctuations limits the resolution of surfactant thickness measurements. A similar limitation is present with neutron reflectivity measurements. Here we have probed $\sim 5 \times 5$ nm² area of the surfactant layer which corresponds to the contact surface of the tip with the surfactant layer.

These techniques do not show the same resolution in adsorbed layer thickness measurements as the force vs separation curves shown in this work. The AFM is the most adequate equipment available for measuring interfacial force with a spatial resolution of few angstroms in the scanned plane and 0.01 nm (thickness resolution measurement) in the normal direction. If we use soft cantilevers with a spring constant of 0.03 N/m, the force resolution in the normal direction to the scanned plane is $0.03 \text{ Nm}^{-1} (0.1 \times 10^{-10} \text{ m}) = 0.3 \text{ pN}$ and by using the dielectric exchange force model it is possible to measure variations in the dielectric permittivity as the one shown in the preceding paragraph, $\Delta \epsilon \approx 0.5$.

The adsorbed surfactant film molecular arrangement with thickness of ~ 5 nm is determined by measurements of the film dielectric permittivity. Before the advent of atomic force microscopy the dielectric permittivity was a macroscopic parameter, appropriate only for describing uniform environments since its profile was difficult to measure for local intermolecular interactions and its spatial distribution was frequently settled without experimental justification. Here, we show that atomic force microscopy made it possible to measure the dielectric permittivity profile in a scale below 5 nm for adsorbed layers of self-assembled surfactant films in water. The DEF models the force acting on the tip during its approach to the interface by assuming a variable dielectric permittivity specific to surfactant adsorbed layers. Since the compactness of the adsorbed film and the conformal structure of the adsorbed molecules, determine the film dielectric permittivity for each pair of values of the layer thickness and dielectric permittivity corresponds only one molecular configuration.

Modeling the force acting on the tip during its immersion in the surfactant layer allows the calculation of the dielectric permittivity at very low frequencies ($f \rightarrow 0$) where all polarization components are present.

IX. CONCLUSIONS

In summary, using AFM, we have investigated the adsorbed structure formed by various cationic surfactants: $C_{16}TAB$, $C_{14}TAB$, $C_{12}TAB$, $2C_{18}DAB$, and CPBr adsorbed on hydrophilic surfaces (mica) immersed in aqueous surfactant solutions. The DEF expression fitted to the force vs separation curve, measured when the tip is immersed in the

adsorbed layer, determines the dielectric permittivity profile with a resolution ~ 0.1 nm. Force measurements were performed in a scale below 5 nm, the molecular nature of the interactions has to be considered. Since the molecular arrangement determines the value of the measured dielectric permittivity of the surfactant film, we were able to obtain direct information about them.

The sensitivity of the technique allows the determination of differences in surfactant molecules' arrangements such as the one measured in CPBr solutions, which corresponds to different compactness of the adsorbed layer associated to the different arrangement of the surfactant molecule aromatic ring.

Our results, then, show distinct molecular configurations in the adsorbed layers as follows: (a) C_{16} TAB surfactant layers' patches formed by a bilayer and a background of monolayers; (b) $2C_{18}$ DAB patches formed by monolayers and an uncovered region; and (c) CPBr bilayers with two different packing densities that result in different dielectric permittivities.

ACKNOWLEDGMENTS

The authors are grateful to J. R. Castro and L. O. Bonugli for technical assistance and acknowledge financial support from FAPESP Grant No. 98/14769-2.

-
- [1] J.P. Rabe, in *Nanostructures Based on Molecular Materials*, edited by W. Gpel and C. Ziegler (VCH, Weinheim, 1992).
- [2] J.M.H.M. Scheutjens and G.J. Fleer, *J. Phys. Chem.* **84**, 178 (1980).
- [3] P.G. de Gennes and P. Pincus, *J. Phys. (Paris), Lett.* **44**, L241 (1983).
- [4] J. Klafter, J.M. Drake, R. Kopelman, and D.D. Awschalom, in *Dynamics in Small Confining Systems*, edited by J.M. Drake, J. Klafter, R. Kopelman, and D.D. Awschalom (Material Research Society, Pittsburgh, 1993).
- [5] J. Klafter and M. Urbakh, *J. Photochem. Photobiol., A* **102**, 29 (1996).
- [6] P.B. Miranda, V. Pflumio, H. Saijo, and Y.R. Shen, *Chem. Phys. Lett.* **264**, 387 (1997).
- [7] A.W. Adamson, *Physical Chemistry of Surfaces* (Wiley, New York, 1990), Chap. XIII.
- [8] J.N. Israelachvili, *Intermolecular and Surface Forces*, 2nd ed. (Academic Press, London, 1992).
- [9] A.M. Gaudin and D.W. Fuerstenau, *Trans. AIME* **202**, 958 (1955).
- [10] J.J. Kipling, *Adsorption from Solution of Non-Electrolytes* (Academic Press, London, 1965).
- [11] P. Chandar, P. Somasundaran, and N.J. Turro, *J. Colloid Interface Sci.* **31**, 117 (1987).
- [12] D.C. McDermott, J. McCarney, R.K. Thomas, and A.R. Rennie, *J. Colloid Interface Sci.* **162**, 304 (1994).
- [13] Y.R. Shen, *Surf. Sci.* **551**, 299 (1994).
- [14] Z.X. Li, J.R. Lu, G. Fragneto, R.K. Thomas, B.P. Blinks, P.D.I. Fletcher, and J. Pentfold, *Colloids Surf., A* **135**, 277 (1998).
- [15] H.N. Patrick and G.G. Warr, *Colloids Surf., A* **162**, 149 (2000).
- [16] F.V. Giesseibl, *Phys. Rev. B* **45**, 13 815 (1992).
- [17] O. Teschke and E.F. de Souza, *Appl. Phys. Lett.* **74**, 1755 (1999).
- [18] O. Teschke and E.F. de Souza, *Rev. Sci. Instrum.* **69**, 3588 (1998).
- [19] I.Y. Sokolov, G.S. Henderson, F.J. Wicks, and G.A. Ozin, *Appl. Phys. Lett.* **70**, 844 (1997).
- [20] S. Manne, J.P. Cleveland, H.E. Gaub, G.D. Stucky, and P.K. Hansma, *Langmuir* **10**, 4409 (1994).
- [21] W.A. Ducker, T.J. Senden, and R.M. Pashley, *Langmuir* **8**, 1831 (1992).
- [22] B. Capella and G. Diether, *Surf. Sci. Rep.* **34**, 1 (1999).
- [23] O. Teschke, G. Ceotto, and E.F. de Souza, *Phys. Rev. E* **64**, 011605 (2001).
- [24] H.J. Butt, *Biophys. J.* **60**, 1438 (1991).
- [25] A.L. Weisenhorn, P. Maivald, H.J. Butt, and P.K. Hansma, *Phys. Rev. B* **45**, 11 226 (1992).
- [26] D.T. Atkins and R.M. Pashley, *Langmuir* **9**, 2232 (1993).
- [27] W.A. Ducker, T.J. Senden, and R.M. Pashley, *Nature (London)* **353**, 239 (1991).
- [28] M. Jaszke, H.J. Butt, S. Manne, H.E. Gaub, O. Hasemann, F. Krinhove, and E.K. Wolff, *Biosens. Bioelectron.* **11**, 601 (1996).
- [29] J.C. Schulz, G.G. Warr, P.D. Butler, and W.A. Hamilton, *Phys. Rev. E* **63**, 041604 (2001).
- [30] B.D. Fleming and E.J. Wanless, *Microsc. Microanal.* **6**, 104 (2000).
- [31] S. Manne and G.G. Warr, in *Supramolecular Structure in Confined Geometries*, edited by S. Manne and G.G. Warr [ACS Symp. Ser. **736**, 2 (1999)].
- [32] S. Manne and H.E. Gaub, *Science* **270**, 1480 (1995).
- [33] S. Manne, *Prog. Colloid Polym. Sci.* **103**, 226 (1997).
- [34] E.J. Wanless and W.A. Ducker, *J. Phys. Chem.* **100**, 3207 (1996).
- [35] E.J. Wanless, T.W. Davey, and W.A. Ducker, *Langmuir* **13**, 4223 (1997).
- [36] R.A. Johnson and R. Nagarajan, *Colloids Surf., A* **167**, 31 (2000).
- [37] R.A. Johnson and R. Nagarajan, *Colloids Surf., A* **167**, 21 (2000).
- [38] O. Teschke and E.F. Souza, *Appl. Phys. Lett.* **74**, 1755 (1999).
- [39] Thermomicroscopes, 1171, Borregas Avenue, Sunnyvale, CA 94089, USA.
- [40] O. Teschke, R.A. Douglas, and T.A. Prolla, *Appl. Phys. Lett.* **70**, 1977 (1997).
- [41] R.M. Sasaki, R.A. Douglas, M.U. Kleinke, and O. Teschke, *J. Vac. Sci. Technol. B* **14**, 2432 (1996).
- [42] L. Bergstrom and E. Bostedt, *Colloids Surf., A* **49**, 183 (1990).
- [43] C.J. Drummond and T.J. Senden, *Colloids Surf., A* **87**, 217 (1994).
- [44] X.Y. Lin, F. Creuzet, and H. Arribart, *J. Phys. Chem.* **97**, 7272 (1993).
- [45] P. Kekicheff, H. Christenson, and B.W. Ninham, *Colloids Surf.* **40**, 31 (1989).

- [46] O. Teschke, G. Ceotto, and E.F. de Souza, *Chem. Phys. Lett.* **326**, 328 (2000).
- [47] U. Kaatze, *J. Solution Chem.* **26**, 1049 (1997).
- [48] O. Teschke, G. Ceotto, and E.F. de Souza, *Phys. Chem. Chem. Phys.* **3**, 3761 (2001).
- [49] S.B. Johnson, C.J. Drummond, P.J. Scales, and S. Nishimura, *Langmuir* **11**, 2367 (1995).
- [50] G. Fragneto, R.K. Thomas, A.R. Rennie, and J. Penfold, *Langmuir* **12**, 6036 (1996).